

# On the mass-metallicity relation, velocity dispersion and gravitational well depth of GRB host galaxies

Maryam Arabsalmani<sup>1,2\*</sup>, Palle Møller<sup>1</sup>, Johan P. U. Fynbo<sup>2</sup>, Lise Christensen<sup>2</sup>,  
Wolfram Freudling<sup>1</sup>, Sandra Savaglio<sup>1,3,4</sup>, Tayyaba Zafar<sup>1</sup>

<sup>1</sup>European Southern Observatory, Karl-Schwarzschild-Strasse 2, 85748 Garching bei München, Germany

<sup>2</sup>Dark Cosmology Centre, Niels Bohr Institute, University of Copenhagen, Juliane Maries Vej 30, DK-2100 Copenhagen Ø, Denmark

<sup>3</sup>Max-Planck-Institut für extraterrestrische Physik, Giessenbachstrasse 1, 85748 Garching bei München, Germany

<sup>4</sup>Physics Department, University of Calabria, via P. Bucci, I-87036 Arcavacata di Rende, Italy

## ABSTRACT

We analyze a sample of 16 absorption systems intrinsic to long duration GRB host galaxies at  $z \gtrsim 2$  for which the metallicities are known. We compare the relation between the metallicity and cold gas velocity width for this sample to that of the QSO-DLAs, and find complete agreement. We then compare the redshift evolution of the mass-metallicity relation of our sample to that of QSO-DLAs and find that also GRB hosts favour a late onset of this evolution, around a redshift of  $\approx 2.6$ . We compute predicted stellar masses for the GRB host galaxies using the prescription determined from QSO-DLA samples and compare the measured stellar masses for the four hosts where stellar masses have been determined from SED fits. We find excellent agreement and conclude that, on basis of all available data and tests, long duration GRB-DLA hosts and intervening QSO-DLAs are consistent with being drawn from the same underlying population.

GRB host galaxies and QSO-DLAs are found to have different impact parameter distributions and we briefly discuss how this may affect statistical samples. The impact parameter distribution has two effects. First any metallicity gradient will shift the measured metallicity away from the metallicity in the centre of the galaxy, second the path of the sightline through different parts of the potential well of the dark matter halo will cause different velocity fields to be sampled. We report evidence suggesting that this second effect may have been detected.

**Key words:** galaxies: high-redshift – galaxies: ISM – galaxies: star formation – galaxies: evolution – galaxies: formation – quasars: absorption lines

## 1 INTRODUCTION

Stellar mass and metallicity are two of the most fundamental physical properties of galaxies. The metal enrichment of the inter stellar medium (ISM) of a galaxy is a consequence of supernova explosions and stellar winds and is therefore related to the star formation history (SFH) of the galaxy. Also, the amount of mass in stars is a function of galaxy SFH. Therefore, understanding the evolution of the two properties and the relation between them is fundamental to understand the formation and evolution of galaxies. Observations have shown that for local and low redshift galaxies a tight relation exists between the galaxy mass and its metallicity (see e.g. Dekel & Woo 2003; Tremonti et al. 2004). The evolution of the mass-metallicity (MZ) relation has been studied using emission lines from HII regions in galaxies out to  $z \gtrsim 3$  and reveal for a galaxy of a given stellar mass a trend of a decreasing metallicity with increasing redshift (Savaglio et al. 2005; Erb et al.

2006; Maiolino et al. 2008; Troncos et al. 2014). Whether the numerous galaxies at the faint end of the luminosity function follow extrapolations of the MZ relation cannot easily be addressed using emission selected samples, and most studies have focused on composite spectra or a few individually selected massive galaxies (Erb et al. 2006; Henry et al. 2013; Cullen et al. 2014). Gravitational lensing which magnifies the flux of background sources is a powerful tool to probe the faint end of the galaxy luminosity function. Studies of low-mass gravitationally lensed galaxies hint at a weaker evolution of the MZ relation and an increasing scatter out to  $z = 2$  (Richard et al. 2011; Wuyts et al. 2012; Christensen et al. 2012; Belli et al. 2013).

Alternative selection techniques to luminosity-limited galaxy samples allow us to form a complementary picture of the MZ evolution with cosmic time (the MzZ relation hereafter, following Christensen et al. (2014)). Long duration Gamma-ray burst (GRB) selected galaxies are preferentially blue, star-forming galaxies (e.g. Le Floch et al. 2003; Christensen et al. 2004) with low metallicities (e.g. Savaglio et al. 2009; Graham et al. 2013). Earlier studies

\* E-mail: marabsal@eso.org

**Table 1.** Sample of 20 GRB host DLA systems with their metallicities and selected low ion lines used for velocity width measurements. Metallicity measurements are based on element X. References for redshifts,  $HI$  column densities, metallicity measurements, and published low-ionization profiles are quoted in the table footnote.

GRB	redshift	$\log [N_{HI}/(cm^{-2})]$	$[X/H]$	X	selected line <sup>a</sup>	Instrument	Ref. <sup>b</sup>
000926	2.0379	$21.3 \pm 0.2$	$-0.13 \pm 0.21$	Zn	SiII 1808	Keck/ESI	(1),(2)
030323	3.3718	$21.90 \pm 0.07$	$-1.26 \pm 0.20$	S	SII 1253	UT4/FORS2	(3)
050401	2.8992	$22.60 \pm 0.30$	$-1.0 \pm 0.4$	Zn	SiII 1808	VLT/FORS2	(4)
050505	4.2748	$22.05 \pm 0.10$	$-1.2 \pm \dots$	S	SiII 1527	Keck/LRIS	(5)
050730	3.9686	$22.10 \pm 0.10$	$-2.18 \pm 0.11$	S	NiII 1370	VLT/UVES	(6)
050820A	2.6147	$21.05 \pm 0.10$	$-0.39 \pm 0.10$	Zn	NiII 1741 <sup>c</sup>	VLT/UVES	(6),(7)
050922C	2.1992	$21.4 \pm 0.3$	$-1.82 \pm 0.11$	Si	FeII 1608	VLT/UVES	(6),(8)
060206	4.0480	$20.85 \pm 0.10$	$-0.84 \pm 0.10$	S	SII 1253	WHT/ISIS	(9)
060510B	4.941	$21.3 \pm 0.1$	$-0.85 \pm 0.15$	S	NiII 1317	Gemini/GMOS	(10)
070802	2.4549	$21.50 \pm 0.20$	$-0.50 \pm 0.68$	Zn	SiII 1808	VLT/FORS2	(11)
071031	2.6922	$22.15 \pm 0.05$	$-1.73 \pm 0.05$	Zn	NiII 1317 <sup>d</sup>	VLT/UVES	(6),(7)
080210	2.641	$21.90 \pm 0.10$	$-1.21 \pm 0.16$	Si	SiII 1808	VLT/FORS2	(12)
081008	1.9683	$21.11 \pm 0.10$	$-0.52 \pm 0.11$	Zn	CrII 2056	VLT/UVES	(13)
090313	3.3736	$21.28 \pm 0.3^e$	$-1.4 \pm 0.3$	Fe+0.3 <sup>f</sup>	MgI 2852	VLT/Xshooter	(14),(15)
090323	3.5690	$20.76 \pm 0.08$	$0.25 \pm 0.09$	Zn	SiII1808	VLT/FORS2	(16)
090926A	2.1071	$21.60 \pm 0.07$	$-1.85 \pm 0.10$	S	FeII 2374	VLT/X-shooter	(17)
100219A	4.6672	$21.14 \pm 0.15$	$-1.1 \pm 0.2$	S	SII 1253	VLT/X-shooter	(14)
111008	5.0	$22.30 \pm 0.06$	$-1.70 \pm 0.10$	S	NiII 1370	VLT/X-shooter	(18)
120327A	2.8145	$21.01 \pm 0.09$	$-1.17 \pm 0.11$	Zn	CrII 2056	VLT/X-shooter	(19)
120815A	2.358	$21.95 \pm 0.10$	$-1.15 \pm 0.12$	Zn	MnII 2594	VLT/X-shooter	(20)

<sup>a</sup>Transition line used to determine the velocity width of low-ionization line profiles.

<sup>b</sup>References: (1) Castro et al. (2003); (2) Savaglio (2006); (3) Vreeswijk et al. (2004); (4) Watson et al. (2006); (5) Berger et al. (2006); (6) Ledoux et al. (2009); (7) This work; (8) Piranomonte et al. (2008); (9) Fynbo et al. (2006); (10) Price et al. (2007); (11) Elíadottir et al. (2009); (12) De Cia et al. (2011); (13) D’Elia et al. (2011); (14) Thöne et al. (2013); (15) de Ugarte Postigo et al. (2010); (16) Savaglio et al. (2012); (17) D’Elia et al. (2010); (18) Sparre et al. (2014); (19) D’Elia et al. (2014); (20) Krühler et al. (2013)

<sup>c</sup>ESO Science Archive, Program Id: 075.A-0385(A), Fynbo et al. (2009)

<sup>d</sup>ESO Science Archive, Program Id: 080.D-0526(A)

<sup>e</sup>J. X. Prochaska, private communication.

<sup>f</sup>Only iron lines are available for this system and we therefore follow the standard procedure (Rafelski et al. 2012) and apply an upward correction of 0.3 dex to the metallicity, to correct for iron depletion and  $\alpha$ -element enhancement.

were biased towards GRBs with bright optical afterglows, and recent unbiased GRB samples (Hjorth et al. 2012) have shown that the hosts follow the general trend of star-forming galaxies at similar redshifts (Michalowski et al. 2012). Damped Lyman- $\alpha$  (DLA) absorption line systems which arise in the GRB host galaxies can be observed out to very high redshifts (e.g. Sparre et al. (2014) analyse the DLA system at  $z \sim 5$  in the GRB 111008A afterglow spectrum and Chornock et al. (2014) obtain metallicity constraints of GRB 140515A at  $z = 6.33$ ) and their metallicity can be measured accurately from absorption lines which arise in the ISM. Since GRB afterglows are transients one can study the host galaxy properties later when the GRB afterglows have faded away. Therefore, GRBs are ideal systems to study the MZ relation and its evolution at high redshifts.

Conventional studies of DLA systems in quasi stellar object (QSO) spectra are used to probe a differently selected population of high redshift galaxies. Metallicities of intervening QSO-DLAs have been measured accurately for several hundred systems at redshifts out to  $z = 5$  (Pettini et al. 1997; Ledoux et al. 2002; Prochaska et al. 2003; Rafelski et al. 2012). However, due to the large difference in magnitudes between the bright background QSOs and the continuum emission from the much fainter foreground galaxies, these are extremely difficult to detect when the line of sight to the galaxy and QSO is very close. This prevents the direct measurement of the stellar masses for most DLA galaxies in

the sightlines of QSOs, and prevents a direct comparative MZ study of this population. To date, only five QSO-DLA galaxies at  $z > 2$  have measured stellar masses (Krogager et al. 2013; Fynbo et al. 2013; Christensen et al. 2014).

While masses of the QSO-DLA galaxies are not known for the majority of the population, the velocity width of low-ionisation species of absorption lines can be used as a proxy for the mass. Indeed, measurements of the velocity widths, defined as  $\Delta v_{90}$ , are shown to correlate with the QSO-DLA metallicities (Ledoux et al. 2006; Prochaska et al. 2008; Møller et al. 2013; Neeleman et al. 2013). In addition, Møller et al. (2013) find evidence for redshift evolution of this correlation, reminiscent of the evolution of the MzZ relation for luminosity-selected galaxies. Simulations demonstrate that galaxies with more massive halos are more likely to produce metal absorption lines in the cold gas of DLA systems with large velocity widths, while small halos produce more of metal absorption lines with low velocity widths (Pontzen et al. 2008; Tescari et al. 2009; Bird et al. 2014) supporting the interpretation of the velocity width-metallicity (VZ) relation as a mass-metallicity (MZ) relation for QSO-DLAs. In what follows we shall therefore use both VZ and MZ, chosen for clarity in the given context, to describe the relation. Whether a VZ relation also holds true for GRB-DLA galaxies is not yet known. Prochaska et al. (2008) analyse four GRB host galaxies, and while the four galaxies are in the

VZ locus of QSO-DLAs, the small sample size does not allow a conclusion about the existence of a VZ relation for GRB-DLAs.

Although both QSO-DLAs and GRB-DLAs are defined based on the large column density of neutral hydrogen, they are selected in different ways; GRB-DLA systems are selected based on the star formation rate (SFR) of the galaxy hosts, while QSO-DLAs are absorption cross-section selected galaxies (Møller and Waren 1998; Fynbo et al. 1999; Prochaska et al. 2008). Hence, they could be drawn from distinct populations of high-redshift galaxies and it is not known whether an MZ relation holds for GRB-DLA systems.

The aim of this paper is to investigate the VZ correlation for a complete literature sample of GRB-DLA galaxies, and place that into context with the relation from QSO-DLAs. Throughout this paper, when we refer to GRBs they are always long duration GRBs.

The paper is organized in the following way. The sample selection is given in section 2. We discuss the velocity width and the effect of spectral resolution in subsections 2.2 and 2.3. In subsection 2.4, the final sample is presented. Our results on the VZ relation for GRB-DLAs and several aspects of comparisons between GRB host galaxies and QSO-DLAs are presented in section 3. A summary of this work and our conclusions are given in section 4.

## 2 DATA

### 2.1 Sample selection

In order to compile a GRB host DLA sample suitable for comparison to the existing samples of QSO-DLAs, we follow Møller et al. (2013) and search the literature for DLA systems in optical spectra of GRBs. In order to be included in our sample the DLA must fulfill the following requirements:

- 1)  $\log N_{HI} \geq 20.3 \text{ cm}^{-2}$
- 2) it must be intrinsic to the GRB host
- 3) it must have a reported absorption metallicity
- 4) it must have at least one unsaturated low ionization line with signal-to-noise appropriate for determination of velocity width.

We find a total of 20 DLAs fulfilling all criteria, and they make up our complete literature sample spanning the redshift range from  $z = 1.97$  to  $z = 5.0$  (Table 1). Five of the systems have high resolution observations (VLT/UVES,  $\text{FWHM} \sim 7 \text{ km s}^{-1}$ ), 8 medium ( $\text{FWHM} \sim 30 - 60 \text{ km s}^{-1}$ ), and 7 low resolution ( $\text{FWHM} \sim 110 - 480 \text{ km s}^{-1}$ ).

### 2.2 Velocity width

To ease comparison with previous work, we use the definition of velocity width given in Prochaska & Wolfe (1997) which is the velocity interval that contains 90% of the area under the apparent optical depth spectrum ( $\Delta v_{90}$ ). We follow Ledoux et al. (2006) and Møller et al. (2013) for the line selection rules and measuring method. The lines we select to measure  $\Delta v_{90}$  for GRB-DLAs in our sample are listed in Table 1.

The accuracy of  $\Delta v_{90}$  measurements critically depends on the resolution of the spectra. Quasar DLA absorption line analysis is effectively only carried out on spectra with resolution high enough that the absorption line profiles are well sampled. Due to the rapid fading of GRB optical transients (OTs), most often we do not have the luxury of high resolution spectra, and we must instead use spectra of lower resolution. Observing at low resolution causes a smearing of the absorption lines which will in turn lead to a measurement of  $\Delta v_{90}$  which is larger than the true  $\Delta v_{90}$ . The magnitude of the

**Table 2.** High resolution line profiles used to correct  $\Delta v_{90}$  for low/medium resolution line profiles

Quasar/GRB	$z_{\text{DLA}}$	$\lambda^a$	$\Delta v_{90}$	Instrument	Ref. <sup>b</sup>
B 2355-106	1.172	2852	129	VLT/UVES	(1)
J 1201+2117	3.798	1808	485	Keck/Hires	(2)
Q 0449-1645	1.007	1862	200	VLT/UVES	(3)
Q 0454+039	0.860	2260	112	VLT/UVES	(4)
J 1107+0048	0.740	2852	178	VLT/UVES	(5)
J 0256+0110	0.725	2852	355	VLT/UVES	(5)
GRB 050730	3.969	1618	26	VLT/UVES	(6)
GRB 050820A	2.615	1608 <sup>c</sup>	307	VLT/UVES	(7)
GRB 050922C	2.199	1608	89	VLT/UVES	(8)
GRB 071031	2.692	1559	51	VLT/UVES	(9)

<sup>a</sup>Rest-frame wavelength of transition lines smoothed to low/medium resolutions.

<sup>b</sup>References: (1) Ellison et al. (2012); (2) Rafelski et al. (2012); (3) Peroux et al. (2008); (4) Pettini et al. (2000); (5) Peroux et al. 2006; (6) Ledoux et al. (2009); (7) This work; (8) Piranomonte et al. (2008); (9) Fox et al. (2008).

<sup>c</sup> ESO Science Archive, Program Id: 075.A-0385(A)

effect depends on both the true  $\Delta v_{90}$  and the resolution of the spectrum. If the true width is large then even very low resolution spectra may still be used, if the true width is very small then the width information may have been lost completely even in a medium resolution spectrum and hence only an upper limit for the velocity width can be derived. For each resolution there is a range of line widths where the effect of the smearing can be computed and corrected for. Prochaska et al. (2008) showed how such a correction could be carried out for observations with  $\text{FWHM} = 45 \text{ km s}^{-1}$  resolution. Here we seek to generalize this method for a large range of resolutions.

### 2.3 Velocity width correction

First we examine our data set and identify the resolution (FWHM) of each of the different instrument/setting configurations used (listed in Table 3). Next we search the literature and select several high resolution (VLT/UVES or Keck/Hires) observed line profiles (Table 2) with  $\Delta v_{90}$  covering a wide range of widths ( $\sim 25 - 485 \text{ km s}^{-1}$ ). The velocity widths of those high-resolution profiles are considered to be the true line widths. We then smooth each of the high resolution lines to each of the lower resolutions (to smooth a line, we convolve it with a Gaussian with  $\sigma$  related to the lower resolution) and measure the  $\Delta v_{90, \text{smooth}}$ . In Fig. 1 (left panel) we plot the resulting widths of the smoothed lines versus their true widths for 5 representative resolutions, using different symbols (and colour coded in the online version) for each resolution. We find that a simple hyperbola of the form

$$\Delta v_{90, \text{smooth}} = (\Delta v_{90, \text{true}}^2 + a^2)^{0.5} \quad (1)$$

where  $a = 1.40 \times \text{FWHM}$ , provides an excellent fit in all cases. The best fit curves of the form given in equation 1 (determined by using a nonlinear least-squares algorithm) are shown in Figure 1. We can now use those fitted curves as a prescription to correct our medium and low resolution data back to their intrinsic values. As pointed out above, the correction can only be trusted if the resolution FWHM is not large enough to completely dominate over the intrinsic width of the line. In case the intrinsic width is equal to the resolution then the measured width will be a factor  $\approx \sqrt{2}$  larger, which is fully possible to correct for. We have therefore chosen

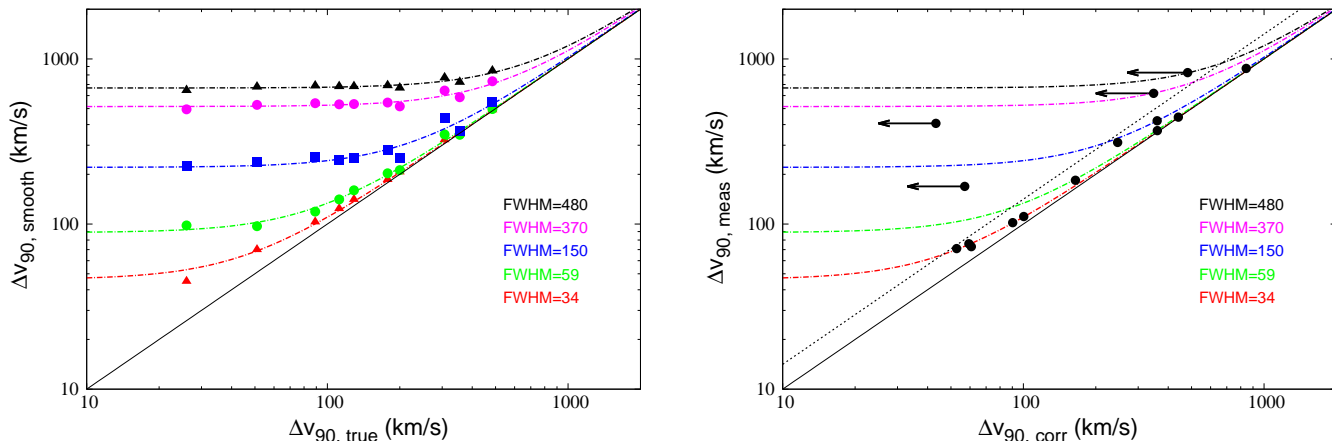


**Figure 1.** Left panel:  $\Delta v_{90}$  of the smoothed line profiles given in Table 2 versus  $\Delta v_{90}$  of the original profiles. Dash-dotted curves show the effect of smoothing to low resolution data as explained in section 2.2. The solid black line marks  $\Delta v_{90,smooth} = \Delta v_{90,true}$ ; Right panel: Dash-dotted curves and full line are the same as in left panel. The dotted line marks  $r = 0.4$  (see section 2.3). Filled circles are the measured values for medium/low resolution lines in our sample. Four points are to the left of  $r = 0.4$  so we obtain only upper limit for their intrinsic widths (see Table 3).

a conservative approach to only trust corrections if the measured width is less than 1.4 times the width after correction. In other words, we define a parameter  $r$  such that

$$r := \frac{\Delta v_{90,meas} - \Delta v_{90,corr}}{\Delta v_{90,corr}}. \quad (2)$$

and only consider systems correctable if  $r \leq 0.4$ . The line corresponding to  $r = 0.4$  is shown as a dotted straight line in Figure 1 (right hand panel). It is seen that four systems are to the left side of the  $r = 0.4$  line, on the flat, uncorrectable part of the curves. These four systems are consequently excluded from further analysis when  $\Delta v_{90}$  is involved.

## 2.4 Final sample

In Table 3 we provide  $\Delta v_{90}$  before and after correction, and also  $r$  values for the 20 DLAs in our sample. For four DLA systems (GRBs 030323, 050401, 050505 and 070802) we cannot reliably correct  $\Delta v_{90}$  and do not include them in any further analysis which involve  $\Delta v_{90}$ . Our final sample consists of 16 GRB host galaxies, spanning the redshift range from  $z = 1.97$  to  $z = 5.0$ .

## 3 ARE GRB HOST GALAXIES AND DLA GALAXIES THE SAME?

### 3.1 Mass-Metallicity relation

DLAs are most commonly observed in the spectra of QSOs, and a large body of data is available in the literature for such DLAs. In this section we investigate whether there is any evidence that the MZ relation of the GRB host galaxies differs from that of QSO-DLAs. For that purpose, we compare the VZ data of GRB hosts presented in section 2 to the QSO-DLA data presented by Møller et al. (2013).

In the upper panel of Figure 2 we present a plot of the two data sets. It can be seen that the observed metallicities fully overlap. A least-square fit of a straight line to both of the data sets individually, shows that the parameters of the fits are identical to within the uncertainties. For the further analysis, we adopt the slope of 1.46 for

**Table 3.** Final results for velocity widths of the GRB-DLA sample

GRB	$\Delta v_{90,meas}$ ( $km s^{-1}$ )	$\Delta v_{90,corr}$ ( $km s^{-1}$ )	$r$	line resolution ( $km s^{-1}$ )
High Resolution				
050730	34	34	...	...
050820A	300	300	...	...
050922C	89	89	...	...
071031	86	86	...	...
081008	60	60	...	...
Medium Resolution				
000926	368	362	0.022	54
060206	444	441	0.008	39
090313	184	165	0.118	59
090926A	71	53	0.344	34
100219A	76	59	0.280	34
111008	111	100	0.106	34
120327A	102	90	0.130	34
120815A	73	61	0.202	29
Low Resolution				
030323	169	$\leq 57$	1.963	114
050401	619	$\leq 348$	0.780	367
050505	407	$\leq 43$	8.398	290
060510B	422	360	0.173	158
070802	826	$\leq 481$	0.716	481
080210	312	247	0.265	137
090323	876	843	0.039	170

The second and third columns are  $\Delta v_{90}$  before and after correction respectively (see equation 1).  $r$  values as defined in equation 2 are given in the fourth column. The resolution (FWHM) of the selected line profiles used for measuring velocity  $\Delta v_{90}$  are given in the fifth column. For four DLA systems (GRBs 030323, 050401, 050505, and 070802)  $r > 0.4$  and hence values of  $\Delta v_{90,corr}$  for these systems are upper limits.

the line, as found by Ledoux et al. (2006), and we fit only intercept for the two samples individually. These fits are shown as full line (GRB hosts) and dotted line (QSO-DLAs) in Figure 2.

### 3.2 Redshift evolution

The MZ relation of QSO-DLA galaxies, as well as that of emission line galaxies, evolves with redshift. Our current sample is too small to independently derive a model for the redshift evolution. However, it is possible to investigate whether the data is consistent with any previously proposed model for the redshift evolution (MzZ). For each MzZ model we use

$$[X/H] = [X/H]_e + f(z) \quad (3)$$

to compute an evolution corrected metallicity ( $[X/H]_e$ ), where  $f(z)$  is the shift in the MZ relation as a function of redshift and  $z$  is the redshift of the galaxy.

We consider three different evolution models. Neeleman et al. (2013) study a sample of DLAs covering the redshift interval from 2 to 5, and report that the MZ relation evolves linearly with a slope of  $-0.32$ . Our first model is to use a line with this slope for the whole redshift range covered by our data as  $f(z)$ .

Based on a study of QSO-DLAs covering the wider redshift interval from 0.1 to 5.1, Møller et al. (2013) find that the MzZ relation of DLAs cannot be well described by a single slope. Rather the relation is constant from the highest observed redshifts to a redshift of 2.6, and evolves then linearly with a slope of  $-0.35$  at lower redshifts. We use this prescription as our second model, and refer to it hereafter as the “late evolution” model. In the lower panel of Figure 2, we show the evolution corrected VZ relation based on the “late evolution” model for both the GRB host and the QSO-DLA samples. The scatter for the evolution corrected relation is lower than that of the uncorrected relation shown in the upper panel. This is a preliminary indication that the GRB host data is consistent with this evolution model.

Finally, Maiolino et al. (2008) investigate the metallicity evolution of emission line selected galaxies. Their data are consistent with linear evolution with a slope of  $-0.35$ . Our third evolution model is again to adopt this slope for evolution throughout our redshift range.

In order to compare the different evolution models, we adopt the following procedure. First, we determine the intrinsic scatter of the VZ relation before and after correcting with each of the evolution models. Following Møller et al. (2013), we separate the total observed scatter  $\sigma_{\text{tot}}$  into contributions from measurement errors  $\sigma_{\text{met}}(i)$  for each GRB host  $i$  and the intrinsic scatter of the relation  $\sigma_{\text{scatter}}$ . For this we define  $C_{\text{dof}}^2$  as

$$C_{\text{dof}}^2 = \sum_{i=1}^{16} \left( ([M/H](i) - 1.46 \log(\Delta v_{90}(i)) - zp) / \sigma_{\text{tot}}(i) \right)^2 / \text{dof}, \quad (4)$$

where  $\sigma_{\text{tot}}(i) = (\sigma_{\text{met}}(i)^2 + \sigma_{\text{scatter}}^2)^{1/2}$ ,  $zp$  is the intercept of the fitted line, and dof is the degrees of freedom, which in this case is 15. We then set  $C_{\text{dof}}$  to its expected value of unity, and numerically solve equation (4) for  $\sigma_{\text{scatter}}$  as a function of  $zp$ . Finally, we adopt the minimum of this function as the value of  $\sigma_{\text{scatter}}$ .

The values found for  $\sigma_{\text{scatter}}$  for each of the evolution models are reported in table 4. The “late evolution” model provides the least intrinsic scatter, and therefore the best fit to the data. From table 4 it is also seen that both “constant slope” models provide larger scatter than the “uncorrected” data. We carry out sets of Monte-Carlo simulations to test the significance of this finding. In each set of simulations, we assume one of the evolution models to be true, and then count the number of times that the intrinsic scatter of the evolution corrected MZ relations computed with different models behave as the real data.

**Table 4.** Redshift evolution models and their effect on the intrinsic scatter of the VZ relation

Redshift evolution model	Observed $\sigma_{\text{scatter}}$	Relative likelihood <sup>a</sup>
late evolution	0.411	1
Constant slope of $-0.32$	0.453	0.060
Constant slope of $-0.35$	0.467	0.035
Uncorrected	0.446	0.255

<sup>a</sup> Relative number of times that the simulation of a model reproduces the observed behaviors in scatter.

The detailed procedure is the following. In each of the simulations, we assign to each GRB host a value for  $[X/H]_e$  based on its redshift using one of the evolution models, and its measured  $\Delta v_{90}$ . We then add normally distributed noise based on the measurement errors  $\sigma_{\text{met}}$ , and additional intrinsic noise  $\sigma_{\text{scatter}}$ . We then compute the observed evolved metallicities with each of the evolution models, and determine  $zp$  and intrinsic scatter as we have done for the real data. For each imposed evolution model, we perform  $10^6$  simulations. We then count the number of times that applying each of the evolution corrections moves the intrinsic scatter as much as the real data do or more.

The relative number of times this happens is reported in table 4. We conclude that if the “late evolution” model is true, it is more than 17 times as likely to observe the scatter behave as observed than if any of the fixed slope evolution models are true. In conclusion of this section, we find that among the 3 models tested, GRB hosts are in better agreement with the late evolution model with a break around  $z \sim 2.6$ .

### 3.3 GRB host metallicities

It has been pointed out that GRB hosts in general have higher observed metallicities than QSO-DLAs at similar redshifts (Fynbo et al. 2006; Savaglio 2006; Prochaska et al. 2007a; Fynbo et al. 2008; Cucchiara et al. 2014). In Figure 3 (left panel) we show the histogram of metallicities (corrected for redshift evolution, i.e. the projection onto the left axis of Figure 2, lower panel) for both GRB hosts and QSO-DLAs. The median metallicity for the two samples is  $-1.19$  and  $-1.53$  respectively, consistent with previous reports. In the right panel we show the corresponding histograms for the  $\Delta v_{90}$ , and it is seen that there also is a corresponding shift of the GRB hosts towards slightly larger velocity widths (median of 95 km/s versus 75 km/s for QSO-DLAs). Seen together the two shifts thus form a shift of the GRB hosts along the relation towards the upper right such that both samples follow the same relation, but the GRB hosts populate the part of the diagram for slightly larger masses than QSO-DLAs. One possible way of understanding this could be that QSO-DLAs and GRB hosts are selected in two different ways from the same underlying sample. Following Fynbo et al. (2008) one may argue that GRB hosts are selected by SFR (as already demonstrated by Christensen et al. (2004)), i.e. weighted  $\propto L$  (luminosity), while QSO-DLAs are selected by cold gas projected absorption area, i.e.  $\propto R^2$  (gas disk radius squared). We know that  $R^2 \propto L^{2t}$  where  $t$  is the Holmberg parameter (Fynbo et al. 1999), and it is now easy to understand how a shift along the relation may occur. For  $t = 0.5$  there will be no shift, for  $t < 0.5$  QSO-DLAs will preferentially be found to the lower left relative to GRB hosts, while for  $t > 0.5$  they will in

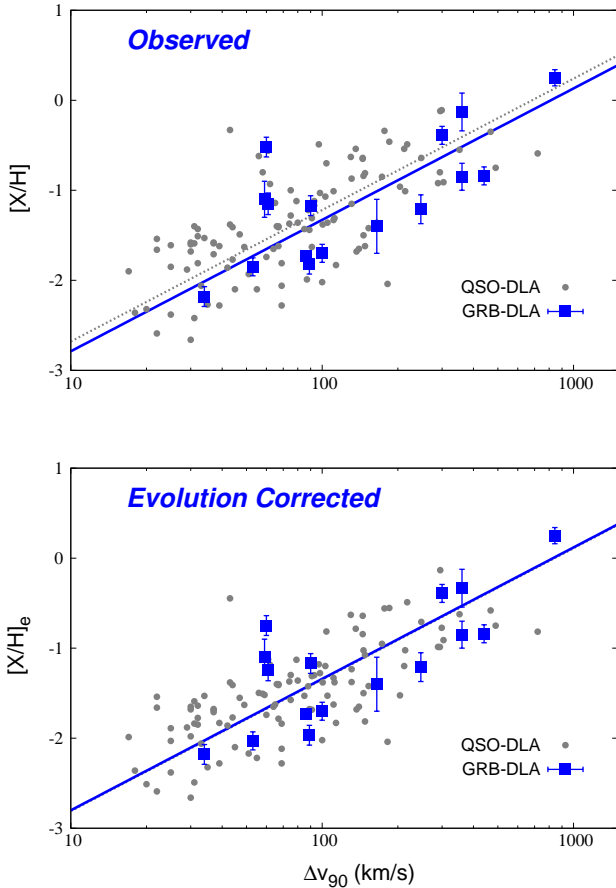


**Figure 2.** Metallicity vs velocity width for QSO-DLAs (small dots) and GRB host DLAs (large blue squares). Upper panel: observed values; Lower panel:  $[X/H]$  values corrected for the redshift evolution determined for QSO-DLAs. For both samples the scatter is reduced indicating that their MZ relations follow similar redshift evolutions. Best fits (using equation 4) are shown as dotted lines (QSO-DLAs), full lines (GRB-DLAs).

general be more Luminous than GRB hosts and therefore be found in the upper right. From Fynbo et al, (1999) we see that  $t$  is 0.4 at  $z = 0$  but that it was smaller (0.25) in the past (at higher redshifts). As a consequence we predict that GRB hosts, on average, will be slightly more massive than QSO-DLAs and that the difference will be larger at higher redshifts. This may be the reason for the metallicity offset reported, but there is an additional effect which may cause GRB hosts to be shifted in the lower plot of Figure 2. The effect is related to the different impact parameter distributions, it is discussed in the following sections and shown in Figure 6. Note that where the effect of selection bias discussed above should only shift along the relation, the effect discussed below is more complex and may possibly result in a shift away from the relation. It is therefore not trivial that the two relations match so well in Figure 2, they could have formed two separate relations.

### 3.4 Impact parameter, metallicity gradient and gravitational well

The one thing we know is different between QSO-DLAs and GRB host DLAs are the sightlines. A QSO-DLA is sampling the HI gas in the intervening DLA galaxy and its halo via random selection.

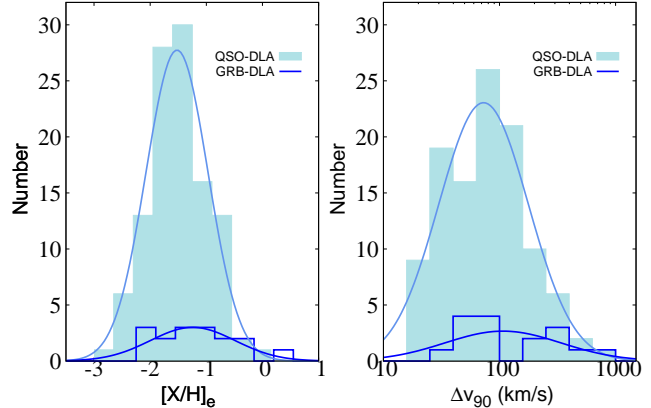


**Figure 3.** Histograms of metallicity and  $\Delta v_{90}$  are presented in left and right panels respectively. The light blue shade show the histograms for the 110 QSO-DLA galaxies (Møller et al. 2013) and the solid dark blue lines are for the 16 GRB-DLA galaxies in our sample (see Tables 1 and 3). Best fit Gaussians are overlotted.

This results in a distribution of impact parameters reflecting the size, shape and inclination of the gas associated with the galaxy (for details see discussion in Møller and Waren 1998). In contrast GRBs are mostly located closer to the centres of their hosts (typically few  $kpc$ ), and therefore they sample gas closer to the centre of the galaxy.

This difference in paths changes the observed spectral lines in three different ways. First the HI column density of GRB-DLAs is higher because of the known impact parameter vs HI column density anti correlation (Møller and Waren 1998; Zwaan et al. 2005; Krogager et al. 2012), second this will have an effect on the measured metallicity if the galaxies have metallicity gradients (van Zee et al. 1998; Swinbank et al. 2012), and third the sightlines will sample different paths through the dark matter gravitational well of the galaxy and they will therefore sample different depths of this gravitational well. We illustrate this in Figure 4. In the bottom panel we see a typical QSO-DLA sightline through the shallow part of the gravitational well, in the top panel the light from a GRB passes from the centre through the deep part of the gravitational well, but only through half of it.

The first point listed above has no effect on our observations, but the other two will move the data points in the VZ plots as explained below.

#### 3.4.1 Metallicity gradient

For easy comparison we correct measured metallicities to the metallicity at the centre of the galaxy. The metallicity gradient of DLA galaxies has been determined observationally to be  $-0.022 \pm 0.004$  dex per  $kpc$  (Christensen et al. 2014), but for QSO-DLAs the impact parameter is mostly unknown, and the authors also give the observationally determined mean correction which is  $0.44 \pm 0.10$ . In Figure 6 we show this "corrected to central" mass metallicity relation for QSO-DLAs.

We search the literature for measurements of impact parameters of the GRBs in our sample but find that only two have been reported (Castro et al. 2003; Thöne et al. 2013). We find that the image of the host has been obtained for an additional GRB (D’Elia et al. 2014) for which we measure the impact parameter. All three values can be found in Table 5. For the impact parameters of the remaining sample we shall use a mean value determined

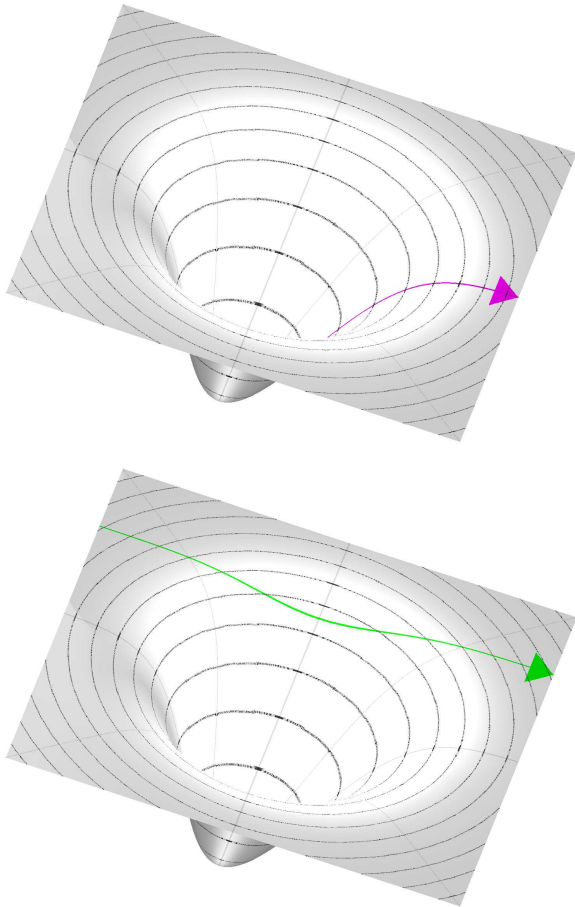


**Figure 4.** Paths of light through the potential well of the host galaxy. The upper panel illustrates a sightline from a GRB that explodes in the centre of the host galaxy, while the lower panel illustrates the random line of sight of a QSO that intersects an intervening galaxy.

from a representative sample of GRB hosts. Such a sample is provided in Bloom et al. (2002) but we find that for a number of the OTs in that sample better astrometry was subsequently provided by Fruchter et al. (2006), and for those we reassess the impact parameters based on the Fruchter et al. (2006) data. From the sample of Perley et al. (2013) we include all GRBs for which coordinates of both hosts and OTs are provided with uncertainty  $\leq 0.3''$ , and for which redshifts are known. The final values of impact parameters are presented in Table 5 and shown in histogram form in Fig 5.

Based on this table we find that the mean, the weighted mean, and the median values are  $2.3 \text{ kpc}$ ,  $2.5 \text{ kpc}$ , and  $2.3 \text{ kpc}$  respectively. All those values are small and very similar and we choose to use the mean value for those hosts with no measured impact parameter. Following Christensen et al. (2014), we use the metallicity gradient of  $-0.022 \text{ dex per kpc}$  and correct the metallicity of the GRB-DLAs in our sample to the central metallicity (Figure 6).

### 3.4.2 Potential well depth

The line of sight to the OT in a GRB host samples only half of the gravitational well in which the host resides (see Figure 4, upper panel). It is hard to predict exactly which value for  $\Delta v_{90}$  one would have observed in case the line had been complete through the other side of the host, but it certainly would not be less than

**Table 5.** List of impact parameters

GRB	Redshift	impact parameter (kpc)	error-bar (kpc)	Reference <sup>a</sup>
GRBs in our sample				
000926	2.038	0.29	0.037	(1)
100219A	4.667	2.6	0.2	(2)
120327A	2.815	3.19	2.39	(3)
other GRBs				
970228	0.695	0.17	0.24	(3)
970508	0.835	0.09	0.09	(4)
970828	0.958	4.05	4.33	(4)
971214	3.418	1.11	0.56	(4)
980425	0.008	2.34	0.01	(4)
980613	1.096	0.78	0.67	(4)
980703A	0.966	0.96	0.54	(4)
990123	1.6	6.11	0.03	(4)
990506	1.31	2.68	4.14	(4)
990510	1.619	0.60	0.08	(4)
990705	0.84	7.17	0.38	(4)
990712	0.434	0.30	0.49	(4)
991208	0.706	0.00	0.62	(3)
991216	1.02	3.12	0.28	(4)
000301C	2.03	0.62	0.06	(4)
000418	1.118	0.20	0.56	(4)
010222	1.477	0.376	0.76	(3)
010921	0.45	2.53	0.52	(3)
011121	0.362	3.98	1.11	(3)
011211	2.141	2.97	2.97	(3)
020405	0.69	5.95	1.57	(3)
020813	1.255	0.18	0.19	(3)
020903	0.251	2.23	2.23	(3)
021004	2.330	0.37	0.37	(3)
021211	1.006	0.71	0.36	(3)
030115	2.5	2.53	1.52	(3)
030329	0.168	0.37	0.13	(3)
040924	0.859	1.70	1.02	(3)
041006	0.716	2.54	1.28	(3)
050915A	2.527	6.72	0.90	(5)
051022	0.8	1.83	1.51	(5)
061222A	2.088	3.12	1.03	(5)
070802	2.455	3.63	1.50	(5)
080325	1.78	5.73	1.04	(5)
080607	3.036	3.30	1.43	(5)
081221	2.26	3.97	0.76	(5)

Redshift of GRBs are given in second column. The third and fourth columns present the impact parameter and corresponding error.

<sup>a</sup> References: (1) Castro et al. (2003); (2) Thöne et al. (2013); (3) this work; (4) Bloom et al. (2002); (5) Perley et al. (2013)

for the observed half galaxy. One could make the simple assumption that the cold clumps in the ISM and halo gas move randomly, but that most are bound inside the gravitational well. In that case  $\Delta v_{90}$  would increase by about a factor  $\sqrt{2}$ . The same type of argument can be applied to sightlines to QSOs through intervening DLA galaxies. Such sightlines will in most cases not pass close to the centre, but rather at impact parameters of order  $\approx 10 \text{ kpc}$  (see Figure 4, lower panel). Again, only a fraction of the full well will be sampled, and the measured  $\Delta v_{90}$  will be smaller than if sampled through the centre. The precise magnitude of those effects is hard to quantify. Detailed high resolution hydro-dynamic simulations would be required to get an estimate.

In Figure 6 we apply the empirical corrections for metallicity gradients, and it is seen that there is now a large shift between

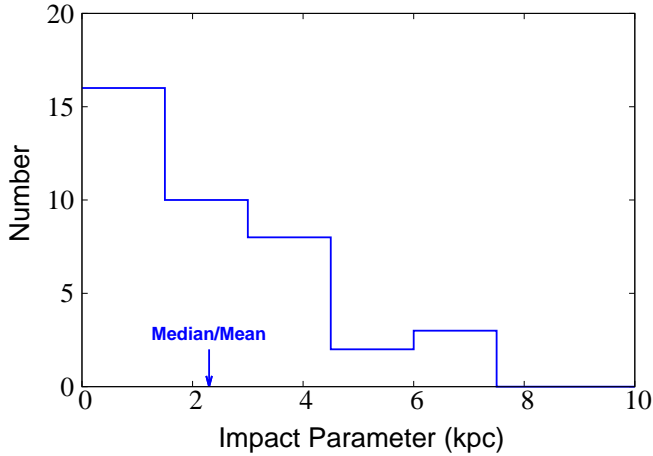


**Figure 5.** Histogram of impact parameters of GRB host galaxies given in Table 5 with both mean and median equal to  $2.3 \text{ kpc}$

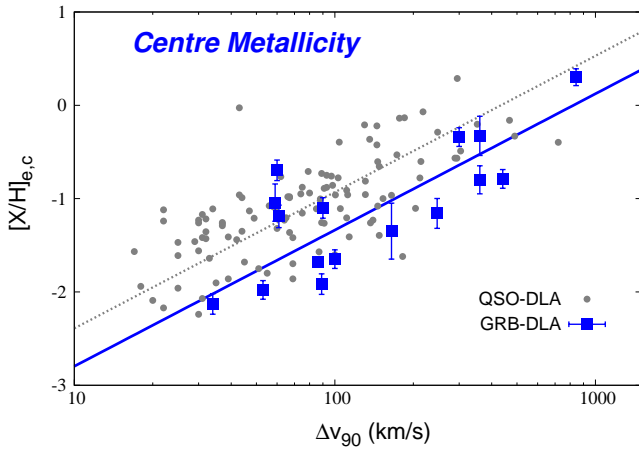


**Figure 6.** Metallicity corrected with the late evolution model and also corrected to the central metallicity ( $[X/H]_{e,c}$ ) vs velocity width for QSO-DLAs (small dots) and GRB host DLAs (large blue squares). Best fits (using equation 4) are shown as dotted lines (QSO-DLAs), full lines (GRB-DLAs).

the two populations. If we interpret this shift as an effect of different sampling of gravitational wells, then the shift corresponds to a factor 2 change of  $\Delta v_{90}$  for galaxies with the same metallicity at a given redshift. The shift is in the sense that QSO-DLAs have  $\Delta v_{90}$  a factor of 2 less than a GRB host with the same metallicity. The shift is therefore in the direction we would expect in case it is due to the gravitational well sampling effect. This may therefore be the effect we have predicted, but at present it is not possible to conclusively prove this.

It is curious, though, that the two samples overlap so perfectly in Figure 2. This means that either there are no metallicity gradients in neither QSO-DLA galaxies, nor in GRB hosts, and also there is no effect due to the gravitational well sampling - or, the effect of metallicity gradients exactly cancels the effect of gravitational well sampling. If the latter is the case then this means that the general concept of an MZ relation plus metallicity gradients simply is a convolved and roundabout way of describing a much simpler underlying relation between metallicity and gravitational well depth.

### 3.5 Stellar mass

A prescription for computation of the stellar mass of QSO-DLA galaxies from only metallicity and redshift was given in Møller et al. (2013). Christensen et al. (2014), improved this prescription by adding the effect of metallicity gradients and also performed a test comparing the computed stellar mass to the measured stellar mass from the SED fits. This test was carried out using the complete set of QSO-DLA galaxies for which the test is currently possible. They concluded that the prescription is confirmed for galaxies of stellar masses down to  $\log(M_*/M_\odot) = 8$ , while for lower stellar masses there are no available data. Here we use the prescription from Christensen et al. (2014) (their equation (3) including the metallicity gradient term  $\Gamma b$ ) to compute the predicted stellar masses of all the host galaxies in our sample (listed in Table 6). For 3 of those, stellar masses have been determined directly via SED fitting (also provided in Table 6). For the host of GRB 090323, we use the photometric data given in McBreen et al. (2010) and determine the stellar mass following the procedure described in Glazebrook et al. (2004) and the initial mass function given in Baldry & Glazebrook (2003). In order to obtain the full distribution function of the allowed mass, a Monte Carlo simulation re-sampling the photometric errors is done. We measure the stellar mass for this host to be  $\log(M_*/M_\odot) = 11.20 \pm 0.75$ . The large error bar is due to only having upper limits on the rest frame optical photometry.

We find the measured stellar masses for these four hosts to be in complete agreement with our computed values provided we use the prescription including the metallicity gradient. If we instead use equation (1) from Christensen et al. (2014), which assumes a constant offset between absorption metallicity and emission metallicity, then the agreement is much poorer with the computed masses in the mean being 1 dex higher than the measured stellar masses. I.e. our data support the hypothesis that the stellar masses of GRB-DLA galaxies follow the same prescription as do QSO-DLA galaxies, and that they have metallicity gradients with a slope similar to that of QSO-DLAs.

In a related study of a sample of 18 low redshift GRB hosts with measured emission line metallicities and stellar masses from SED fits, Mannucci, Salvaterra, & Campisi (2011) showed that those host galaxies follow the same M-Z relation as SDSS galaxies, but only after correcting for the high SFR which is a result of the SFR weighted selection we discussed in section 3.3. It therefore appears that the available samples of emission selected galaxies, GRB selected galaxies, and DLA selected galaxies follow the same M-Z relations (when corrected for their specific selection function) and likely are drawn from the same underlying galaxy sample.

In Section 3.3 we described how the metallicity offset seen in Figure 3 could be understood as a result of selection functions, but from Figure 6 it is seen that the offset could just as well be caused by the effect of metallicity gradients and different impact parameter distributions. Our sample covers a range of stellar masses from  $10^{6.7}$  to  $10^{11} M_\odot$ , with a median of  $10^{8.5}$  (Table 6). This median mass is identical to that reported by Møller et al. (2013) for DLA galaxies which, held together with the better fits using metallicity gradients described above, supports that at least part of the metallicity offset is a result of different impact parameter distributions. In that case the shift between the two samples seen in Figure 6 is most easily interpreted as the effect of different paths through the gravitational potentials.

The interpretation of the observed distribution of data points in Figure 2 is therefore complex. Effects of redshift evolution,



**Table 6.** For the sample of the GRB-DLA galaxies, redshift, impact parameter, and metallicity are presented in second, third, and fourth columns respectively. Predicted and measured stellar masses are given in the fifth and sixth columns.

GRB	redshift	$b$ (kpc)	$[X/H]$	Predicted mass, $\log(M_*/M_\odot)$	Measured mass, $\log(M_*/M_\odot)$
000926	2.0379	0.29	$-0.13 \pm 0.21$	$9.91 \pm 0.81$	$9.52 \pm 0.84$
030323	3.3718	...	$-1.26 \pm 0.20$	$8.34 \pm 0.80$	...
050401	2.8992	...	$-1.0 \pm 0.4$	$8.80 \pm 1.01$	...
050505	4.2748	...	$-1.2 \pm \dots$	$8.45 \pm > 0.72$	...
050730	3.9686	...	$-2.18 \pm 0.11$	$6.73 \pm 0.75$	...
050820A	2.6147	...	$-0.39 \pm 0.10$	$9.88 \pm 0.74$	$8.64^{+0.58}_{-0.23}$
050922C	2.1992	...	$-1.82 \pm 0.11$	$7.11 \pm 0.75$	...
060206	4.048	...	$-0.84 \pm 0.10$	$9.08 \pm 0.74$	...
060510B	4.941	...	$-0.85 \pm 0.15$	$9.07 \pm 0.77$	...
070802	2.4549	3.63	$-0.50 \pm 0.68$	$9.64 \pm 1.40$	$9.7^{+0.2}_{-0.3}$
071031	2.6922	...	$-1.73 \pm 0.05$	$7.52 \pm 0.73$	...
080210	2.641	...	$-1.21 \pm 0.16$	$8.43 \pm 0.78$	...
081008	1.9683	...	$-0.52 \pm 0.11$	$9.26 \pm 0.75$	...
090313	3.3736	...	$-1.40 \pm 0.30$	$8.10 \pm 0.90$	...
090323	3.569	...	$0.25 \pm 0.09$	$11.00 \pm 0.74$	$11.20 \pm 0.75$
090926A	2.1071	...	$-1.85 \pm 0.10$	$7.00 \pm 0.74$	...
100219A	4.6672	2.6	$-1.10 \pm 0.20$	$8.64 \pm 0.80$	...
111008	5.0	...	$-1.70 \pm 0.10$	$7.57 \pm 0.74$	...
120327A	2.8145	3.19	$-1.17 \pm 0.11$	$8.54 \pm 0.75$	...
120815A	2.358	...	$-1.15 \pm 0.12$	$8.39 \pm 0.75$	...

References for measured stellar masses: Savaglio et al. (2009) for 000926; Chen et al. (2009) for 050820A; Krühler et al. (2011) for 070802; This work for 090323.

impact parameter distributions, metallicity gradients, and differently weighted selection functions all work to move the data-points, which causes at least part of the scatter of the relation. We here repeat from the conclusions of Møller et al. (2013) that in order to move forward towards an understanding of those objects we need to identify and understand the sources of the scatter. One of the sources (redshift evolution) has already been identified. Christensen et al. (2014) recently found that half of the scatter in their sample was removed when the effect of metallicity gradients were included. Here we have proposed that the effect of gravitational well depth could be an additional cause of scatter.

#### 4 CONCLUSIONS

Most long duration GRB host galaxies display strong intrinsic DLA absorption systems similar in nature to the intervening DLA systems seen in QSO spectra. The GRB host systems are, however, different in two ways: they originate inside the host galaxies rather than behind them and they are found at much smaller impact parameters. In addition they are also reported generally to have higher HI column densities and often to have higher metallicities than intervening DLAs at the same redshift.

It is important to establish if those differences simply are a result of two different selection functions applied to the same underlying sample of high redshift galaxies, or if the two types of galaxies are truly two different populations.

We have here analysed the mass/metallicity/redshift relations of a complete literature sample of GRB host galaxies and a sample of intervening DLA galaxies in order to address this question. We have found that

1) The two samples are fully consistent with being drawn from the same underlying population with a single MZ relation, and a sin-

gle redshift evolution of this relation with a break around  $z \approx 2.6$ . GRB hosts are in better agreement with this redshift evolution compared to linear evolutions with constant slopes.

2) There is evidence that the GRB host galaxies have higher metallicities, but this is most likely a secondary correlation. The primary correlation is with either impact parameter, with stellar mass, or, presumably, with a combination of the two. The smaller impact parameters combined with a metallicity gradient will produce a metallicity offset, SFR selection bias is predicted to select galaxies of somewhat larger stellar mass than DLA galaxies which will likewise cause an offset in metallicity.

3) There is weak evidence that the  $\Delta v_{90}$ -metallicity relation for the GRB hosts is offset towards larger  $\Delta v_{90}$  values, as one would predict since their sightlines pass through a deeper part of the dark matter halo potential well than a random sightline to an intervening DLA in a halo of the same mass.

It has been shown previously that QSO-DLAs and Lyman Break Galaxies (LBG) are consistent with being drawn from the same underlying population by two very different selection functions, where QSO-DLAs are drawn from the very low-mass end of the LBG population (Møller et al. 2002). With the results presented here we have now added long duration GRB hosts to this list, which means that we have made another important step towards a global description of galaxies and galaxy evolution in the early universe.

Since the sample used in this pilot study is limited, it will be quite feasible to improve the accuracy of all results reported here simply by increasing the sample size. GRB host are ideally suited to shed light on the structure of high redshift galaxies. They combine the data from emission selected galaxies directly with those of absorption selected galaxies. I.e. we obtain in the ideal case both absorption metallicity, emission metallicity, stellar mass from SED fits, impact parameter and  $\Delta v_{90}$  for a single galaxy.

**ACKNOWLEDGMENT**

We would like to thank Jason X. Prochaska for providing the HI column density for the host of GRB 090313 prior to publication. We thank an anonymous referee for a careful reading of our manuscript and for many insightful and valuable comments which significantly improved the presentation of our results. We thank Karl Glazebrook and Damien Le Borgne for helping with the stellar mass calculation of the host of GRB 090323. MA thanks Max-Planck-Institut für Astrophysik for hosting her during the initial part of this work. JPUF acknowledges support from the ERC-StG grant EGGS-278202. This work was funded by an ESO DGDF grant to PM and WF. The Dark Cosmology Centre is funded by the Danish National Research Foundation.

**REFERENCES**

- Asplund M., Grevesse N., Sauval A.J., Scott P., 2009, *ARA&A*, 47, 481
- Baldry I.K., Glazebrook K., 2003, *ApJ*, 593, 258
- Belli S., Jones T., Ellis R.S., Richard J., 2013, *ApJ*, 772, 141
- Berger E., Penprase B.E., Cenko S.B., Kulkarni S.R., Fox D.B., Steidel C.C., Reddy N.A., 2006, *ApJ*, 642, 979
- Bird S., Haehnelt M., Neeleman M., Genel S., Vogelsberger M., Hernquist L., 2014, arXiv1407.7858B
- Bloom J.S., Kulkarni S.R., Djorgovski S.G., 2002, *ApJ*, 123, 1111
- Castro S., Galama T.J., Harrison F.A., Holtzman J.A., Bloom J.S., Djorgovski S.G., Kulkarni S.R., 2003, *ApJ*, 586, 128
- Chen H. et al., 2009, *ApJ*, 691, 152
- Christensen L., Møller P., Fynbo J.P.U., Zafar T., 2014, arXiv1404.6529
- Christensen et al., 2012, *MNRAS*, 427, 1973
- Christensen L., Hjorth J., Gorosabel J., 2004, *A&A*, 425, 913
- Chornock R., Berger E., Fox D.B., Fong W., Laskar T., Roth K.C., 2014, arXiv1405.7400
- Cucchiara A., Fumagalli M., Rafelski M., Kocevski D., Prochaska J.X., Cooke R.J., Becker G.D., 2014, arXiv1408.3578
- Cullen F., Cirasuolo M., McLure R.J., Dunlop J.S., Bowler R.A.A., 2014, *MNRAS*, 440, 2300
- De Cia A. et al., 2011, *MNRAS*, 412, 2229
- D'Elia V. et al., 2014, *A&A*, 564, 38
- D'Elia V., Campana S., Covino S., D'Avanzo P., Piranomonte S., Tagliaferri G., 2011, *MNRAS*, 418, 680
- D'Elia V. et al., 2010, *A&A*, 523, 36
- Dekel A., Woo J., 2003, *MNRAS*, 344, 1131
- de Ugarte Postigo A. et al., 2010, *A&A*, 513, 42
- Elíadóttir A. et al., 2009, *ApJ*, 697, 1725
- Ellison S. L., Kanekar N., Prochaska J.X., Momjian E., Worseck G., 2012, *MNRAS*, 424, 293
- Erb D.K., Shapley A.E., Pettini M., Steide, C.C., Reddy N.A., Adelberger K.L., 2006, *ApJ*, 644, 813
- Fox A.J., Ledoux C., Vreeswijk P.M., Smette A., Jaunsen A.O., 2008, *A&A*, 491, 189
- Fruchter A.S. et al., 2006, *Natur*, 441, 463
- Fynbo, J.P.U. et al., 2013, *MNRAS*, 436, 361
- Fynbo J.P.U. et al., 2009, *ApJSS*, 185, 526
- Fynbo J.P.U., Prochaska J.X., Sommer-Larsen J., Dessauges-Zavadsky M., Møller P., 2008, *ApJ*, 683, 321
- Fynbo J.P.U. et al., 2006, *A&A*, 451, 47
- Fynbo J.P.U., Møller P., Warren S.J., 1999, *MNRAS*, 305, 849
- Glazebrook k. et al., 2004, *Natur*, 430, 181
- Graham J.F., Fruchter A.S., 2013, *ApJ*, 774, 119
- Henry A. et al., 2013, *ApJ*, 776, 27H
- Hjorth J. et al., 2012, *ApJ*, 756, 187
- Krogager J.-K. et al., 2013, *MNRAS*, 433, 3091
- Krogager J.-K., Fynbo J.P.U., Møller P., Ledoux C., Noterdaeme P., Christensen L., Milvang-Jensen B., Sparre M., 2012, *MNRAS*, 424, 1
- Krühler et al., 2013, *A&A*, 557, 18
- Krühler et al., 2011, *A&A*, 534, 108
- Ledoux C., Vreeswijk P.M., Smette A., Fox A.J., Petitjean P., Ellison S.L., Fynbo J.P.U., Savaglio S., 2009, *A&A*, 506, 661
- Ledoux C., Petitjean P., Fynbo J.P.U., Møller P., Srianand R., 2006, *A&A*, 457, 71
- Ledoux C., Bergeron J., Petitjean P., 2002, *A&A*, 385, 802
- Le Floch E. et al., 2003, *A&A*, 400, 499
- Maiolino R., et al., 2008, *A&A*, 488, 463
- Mannucci F., Salvaterra R., Campisi M.A., 2011, *MNRAS*, 414, 1263
- Michaleowski M.J. et al., 2012, *ApJ*, 755, 85
- McBreen S. et al., 2010, *A&A*, 516, 71
- Møller P., Fynbo J.P.U., Ledoux C., Nilsson K.K., 2013, *MNRAS*, 430, 2680
- Møller P., Warren S.J., Fall S.M., Fynbo J.P.U., Jakobsen P., 2002, *ApJ*, 574, 51
- Møller P., Warren S.J., 1998, *MNRAS*, 299, 661
- Neeleman M., Wolfe A.M., Prochaska J.X., Rafelski M., 2013, *ApJ*, 769, 54
- Perley D.A. et al., 2013, *ApJ*, 778, 128
- Péroux C., Meiring J.D., Kulkarni V.P., Khare P., Lauroesch J.T., Vladilo G., York D.G., 2008, *MNRAS*, 386, 2209
- Péroux C., Meiring J.D., Kulkarni V.P., Ferlet R., Khare P., Lauroesch J.T., Vladilo G., York, D.G., 2006, *MNRAS*, 372, 369
- Pettini M., Ellison S.L., Steidel C.C., Shapley A.E., Bowen D.V., 2000, *ApJ*, 532, 65
- Pettini M., Smith L.J., King D.L., Hunstead R.W., 1997, *ApJ*, 486, 665
- Piranomonte S. et al., 2008, *A&A*, 492, 775
- Pontzen A. et al. 2008, *MNRAS*, 390, 1349
- Price P.A. et al., 2007, *ApJ*, 663, 57
- Prochaska J.X., Chen H., Wolfe A.M., Dessauges-Zavadsky M., Bloom J.S., 2008, *ApJ*, 672, 59
- Prochaska J.X., Chen H., Dessauges-Zavadsky M., Bloom J.S., 2007a, *ApJ*, 666, 267
- Prochaska J.X. et al., 2007b, *ApJS*, 168, 231
- Prochaska J.X., Gawiser E., Wolfe A.M., Castro S., Djorgovski S.G., 2003, *ApJ*, 595, 9
- Prochaska J.X., Wolfe A.M., 1997, *ApJ*, 487, 73
- Rafelski M., Wolfe A.M., Prochaska J.X., Neeleman M., Mendez A.J., 2012, *ApJ*, 755, 89
- Richard J., Jones T., Ellis R., Stark D.P., Livermore R., Swinbank M., 2011, *MNRAS*, 413, 643
- Savaglio S. et al., 2012, *MNRAS*, 420, 627
- Savaglio S., Glazebrook K., Le Borgne D., 2009, *ApJ*, 691, 182
- Savaglio S., 2006, *NJP*, 8, 195
- Savaglio S. et al., 2005, *ApJ*, 635, 260
- Savaglio S., Fall S.M., Fiore F., 2003, *ApJ*, 585, 638
- Sparre et al., 2014, *ApJ*, 785, 150
- Swinbank A.M., Sobral D., Smail Ian, Geach J.E., Best P.N., McCarthy I.G., Crain R.A., Theuns T., 2012, *MNRAS*, 426, 935
- Tescari E., Viel M., Tornatore L., Borgani S., 2009, *MNRAS*, 397, 411
- Thöne C.C. et al., 2013, *MNRAS*, 428, 3590

Tremonti et al. 2004, ApJ, 613, 898  
Troncoso P., et al., 2014, A&A, 563, 58  
van Zee L., Salzer J.J., Haynes M.P., O'Donoghue A.A., Balonek  
T.J., 1998, AJ, 116, 2805  
Vreeswijk P.M. et al., 2004, A&A, 419, 927  
Watson D. et al., 2006, Apj, 652, 1011  
Wuyts E., Rigby J.R., Sharon K., Gladders M.D., 2012, ApJ, 755,  
73  
Zwaan M.A., van der Hulst J.M., Briggs F.H., Verheijen M.A.W.,  
Ryan-Weber E.V., 2005, MNRAS, 364, 1467

This paper has been typeset from a  $\text{\TeX}/\text{\LaTeX}$  file prepared by the  
author.